Research Article

Nur Athirah Sukrey, Muhammad Rizwan, Abd Razak Bushroa*, Siti Zuliana Salleh, and Wan Jefrey Basirun

Development and characterization of bioglass incorporated plasma electrolytic oxidation layer on titanium substrate for biomedical application

https://doi.org/10.1515/rams-2021-0052
received May 05, 2021; accepted July 08, 2021

Abstract: In this research, the growth of bioglass (BG) (45S5) incorporated oxide layer via plasma electrolytic oxidation (PEO) method was studied with respect to different sodium hydroxide (NaOH) concentrations (0.1, 0.3, 0.5, and 0.7 M). The voltage response during the deposition process was highly dependent on the electrolyte concentration. Large sparks were recorded at the lowest electrolyte concentration. The result also showed that the increment of electrolyte concentration improved the thickness and mechanical properties of BG-coated pure titanium (TI) surfaces via the PEO process. However, the morphological investigation showed that the coating formation and the uniformity of coating distribution are dependent on the optimum concentration of the electrolyte. This study demonstrates the feasibility of the PEO method in producing a uniform bio-functional coating for biomedical applications.

Keywords: PEO, BG, electrolyte concentration, adhesion strength, NaOH concentration

*** Corresponding author: Abd Razak Bushroa,** Department of Mechanical Engineering, Faculty of Engineering, Universiti Malaya, 50603 Kuala Lumpur, Malaysia; Department of Mechanical Engineering, Faculty of Engineering, Centre of Advanced Manufacturing and Materials Processing (AMMP), Universiti Malaya, 50603 Kuala Lumpur, Malaysia, e-mail: bushroa@um.edu.my
Nur Athirah Sukrey, Siti Zuliana Salleh: Department of Mechanical Engineering, Faculty of Engineering, Universiti Malaya, 50603 Kuala Lumpur, Malaysia; Department of Mechanical Engineering, Faculty of Engineering, Centre of Advanced Manufacturing and Materials Processing (AMMP), Universiti Malaya, 50603 Kuala Lumpur, Malaysia
Muhammad Rizwan: Department of Metallurgical Engineering, NED University of Engineering and Technology, 75270, Karachi, Pakistan
Wan Jefrey Basirun: Department of Chemistry, Faculty of Science, Universiti Malaya, 50603 Kuala Lumpur, Malaysia

1 Introduction

Titanium (Ti) and its alloys have been widely used in aerospace, petrochemical, architectural, and biomedical industries [1] due to the good mechanical properties, low density, low elastic modulus, high biocompatibility, relatively high melting point, and excellent corrosion resistance [2–4]. Abreast with these wide applications of Ti, researchers are continuously finding robust solutions to improve the mechanical properties for better resilience or flexibility [5], in addition to enhancing the bioactivity and antibacterial activity [6] of Ti and its alloys for biomedical applications.

One of the feasible means to widen the mechanical and bioactivity properties is via the surface treatment for the formation of a protective layer on the Ti alloys [7–9]. Therefore, the incorporation of bioactive materials into the protective layer formed on the Ti surface would promote bioactivity without compensating for the excellent mechanical properties. There is a significant research interest for the development of adherent bioactive layer on Ti-based implant materials due to the inert nature of Ti compared to the other metal surfaces [10,11]. Bioglass (BG) is a bioactive material capable of improving the interaction of the implant material with surrounding body fluid and inducing the formation of an apatite layer at the bone/implant interface [12,13]. Hence, by incorporating a layer of BG material onto a Ti substrate, the desired mechanical and biological properties of a medical implant could be achieved [14,15]. Despite the brittleness reported in regards of the BG incorporated coating, the excellent bioactivity of BG exhibits appealing characteristics for the surface modification of biomedical implant materials [16]. Thus, it is crucial to overcome this mechanical strength limitation without compensating the bioactivity and biocompatibility of BG. Among the commercially available BGs, the 45S5 is widely employed due to the good bioactive coating properties, which bonds with soft and

hard tissues, as well as for bone tissue growth and regeneration [17]. This is related to a direct chemical bond mechanism due to the formation of hydroxyl carbonated apatite on the surface [18] which is initiated by the rapid dissolution of alkali from the glass surface when in contact with aqueous solutions [19,20].

The surface modification of various alloys has been widely studied by utilizing the plasma electrolytic oxidation (PEO) method. The PEO technique is the most preferred coating technique as it does not require complex set up of equipment and produces excellent wear and corrosion resistance, adherence, and uniform bio-functional hydroxyapatite incorporated oxide coatings on the surface of metallic substrates [21,22]. Most of the coating techniques for the deposition of bioactive ceramic layers require a separate sintering step that yields cracking between the substrate and the bioceramic layer. Contrary to these techniques, PEO offers excellent adhesion and microporous layer without particular post heat treatment. The antibacterial properties offered by BG is an added benefit to the surface modification of implant surface [23]. Hence, the deposition of BG-based antibacterial adherent coating on metallic Ti substrates exhibits as a vital research domain [24].

The incorporation of functional bioactive materials by using the PEO technique has been reported in few research articles recently [25,26]. However, the effect of the electrolyte concentration on the structural and mechanical characteristics of BG incorporated PEO coating is still unclear. The low melting point of BG (ranging from 800 to 1,000°C) makes the deposition of BG incorporated coating hard, as suggested by the previous researcher [27]. Moreover, this PEO method is a constantly evolving coating method, proving that it is not an obsolete method of coating [28]. Thus, it is worth reporting a study on the influence of electrolyte concentration with BG addition of PEO coating. Previous work reported the influence of various electrolytes in manipulating the mechanical strength of the produced PEO coating [29]; however, the effect of electrolytes is still unclear. Besides, only few reports regarding BG utilization with sodium hydroxide (NaOH) as an electrolyte for Ti coating are found. It is expected that the concentration of OH^- ions of NaOH will further affect the particles' ionization, thus producing a varied response of BG particles incorporation into the coating. Under this condition, the increase in Na^+ concentration due to the increase in NaOH concentration in PEO electrolyte appreciates the formation of bioactive apatite layer in the simulated body fluid (SBF) immersion test [30–32].

Additionally, the voltage-time response and the mechanical properties of BG incorporated oxide coating produced at different electrolyte concentrations are yet to be examined. Hence, in this study, the behaviour of the PEO deposition was studied as a function of NaOH concentration in an electrolyte suspension containing BG (45S5) composition. The voltage-time response, cross-sectional appearance, and surface morphologies of the PEO films produced under the galvanostatic mode, in addition to the mechanical properties concerning hardness and adhesion strength, and the bioactivity in SBF immersion testing of the formed layer are evaluated in detail. The process is shown in graphical abstract.

2 Experimental methods

2.1 Substrate preparation

A commercially pure Ti (Cenco Sains Special Materials Co. Ltd., Malaysia) coupon of sizes (15 mm × 30 mm × 2 mm) was abraded with silicon carbide abrasive paper of different grit sizes (600, 800, 1,000, 1,200, 1,500, and 2,000) for 2 min before being polished on a polishing cloth with diamond suspension. Subsequently, the abraded and polished coupons were ultrasonically cleaned with distilled water and ethanol bath for 40 min. These surface preparations are crucial to remove the unwanted scratches and contaminants before the PEO treatment process.

2.2 Electrolyte preparation

The ready-to-use BG powder (45S5) (XL Sci-Tech Inc., US) was used as a precursor in the electrolyte in this study. The BG 45S5 contains 24.5 wt% of each CaO and Na_2O along with 6 wt% of P_2O_5 with predominant content of SiO_2 (balance). The presence of phosphate, calcium, and silicate ions is responsible for its highest bioactivity due to the inherent similarity with the bone mineral. The nomenclature 45S5 represents that BG contains 45 wt% of silica, while the molar ratio between calcium and phosphorous is 5 [16]. The detail of each electrolyte composition is shown in Table 1. All the measurements were taken using an electronic balance (OHAUS Adventurer Precision Balancer, US). The electrolyte was mixed and stirred continuously by using a magnetic stirrer plate (Snijders 34532 Hotplate Magnetic Stirrer, Netherlands) and magnetic bar for 1.5 h and subsequently sonicated in the ultrasonic bath for 1 h to ensure the homogenous distribution of the suspension components. The pH of the electrolyte was measured by using a pH meter

Table 1: Composition of electrolyte suspension

Experiment name	C1	C2	C3	C4
Amount of NaOH (g)	1.992	6.075	10.068	14.146
Amount of bioglass (g)	2.510	2.496	2.499	2.499
Amount of distilled water (mL)	500	500	500	500
Molarity (M)	0.10	0.30	0.50	0.70
pH	13.00	13.48	13.70	13.85

(Fisherbrand™ accumet™ AE150 Benchtop pH Meter, US) once the electrolyte preparation was completed.

2.3 PEO deposition process

The prepared Ti coupon was immersed in the electrolyte in a stainless steel beaker (Volume: 500 mL) surrounded with water cooling bath system. The whole PEO set up is shown in Figure 1. The mixer/agitator is critical for the set up in order to avoid agglomeration and sedimentation of the electrolyte during the deposition process. The temperature of the cooling water bath was set at 20°C throughout the process. The PEO deposition process was carried out with the aid of autoranging DC power supply unit (Keysight Technologies Deutschland GmbH, Model No: N8957A, Germany). The parameters for the PEO treatment are shown in Table 2.

Table 2: Electrical parameters used during the PEO deposition process

PEO electrical parameters	Value
Maximum current applied (A)	2
Voltage threshold (V)	350
Deposition time (min)	3

2.4 Coating characterization

2.4.1 Structural characterization

The coating microstructure and morphology was observed by utilizing a field emission scanning electron microscopy (FESEM) (ZEISS SIGMA 300 VP Microscopy, Germany) attached with energy dispersive X-Ray analysis (EDS). The coated sample was mounted onto an epoxy resin mould and cross sectioned for the coating thickness and elemental analysis across the formed oxide layer.

2.4.2 Mechanical characterization

The adhesion strength test was performed on the coated Ti coupon by using a conical Rockwell diamond tip with a radius of 25 µm (Micro Materials Ltd. Wrexham, UK). A linearly increasing load from 0 to 2,000 mN is applied

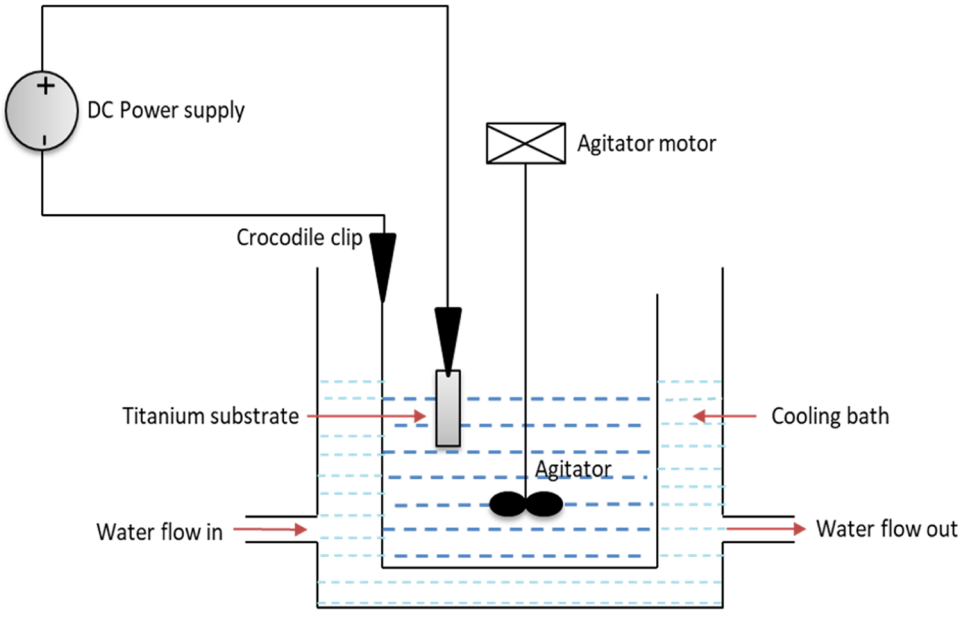

Figure 1: The schematic diagram of PEO set up.

along a 1,000 μm length scratch. The critical load (L_C) causing the coating delamination was evaluated as the failure point. The scratch track was observed via an optical microscope for the failure mode measurement and observation.

2.4.3 Bioactivity testing

The bioactivity of the coating was evaluated by the apatite forming ability of the PEO deposited coating after immersion in the SBF solution. The SBF was prepared according to the Kokubo and Takadama [33] and Kokubo et al. protocols [34], where the ionic concentration of the solution was almost the same as the human body fluid. The solution was prepared by dissolving sodium chloride, NaCl (Ajax Finechem, US), potassium chloride, KCl (EMSURE® Merck KGaA, Germany), magnesium chloride hexahydrate, $MgCl_2.6H_2O$ (Ajax Finechem, US), calcium chloride, $CaCl_2$ (Sigma-Aldrich, US), sodium hydrogen carbonate, $NaHCO_3$ (Sigma-Aldrich, US), potassium hydrogen phosphate trihydrate, $K_2HPO_4.3H_2O$ (Friendemann Schmidt Chemicals, German), sodium sulphate, Na_2SO_4 (Sigma-Aldrich, US), and tris-hydroxymethyl aminomethane, $(CH_2OH)_3CNH_2$ (EMSURE® Merck KGaA, Germany) one after another in 500 mL of distilled water and deionized water. About 40 mL of hydrochloric acid, HCl (Sigma-Aldrich, US) was titrated with the solution with stirring until pH 7.4 was obtained. The preparation of the solution was done in a water bath at 36.5°C with magnetic stirring to ensure the uniform homogeneity of the SBF.

The coated substrate was immersed in about 30 mL of the prepared SBF and incubated at a constant temperature of 37°C for 14 days. After the immersion, the substrate was taken out from the immersion container and washed thoroughly with distilled water before being dried at room temperature. The dried substrate was characterized by FESEM and EDS to confirm the presence of the newly formed apatite layer. The calcium to phosphor (Ca/P) ratio of the apatite layer was evaluated from the elemental distribution in the EDS characterization.

3 Results and discussions

3.1 Mechanism of coating formation via PEO process

The formation of the oxide coating encapsulating the metal substrate can be classified into three stages which are the passive oxide film growth, breakdown of the passive oxide film, and the growth of the oxide film with melted substrate material that occurs repetitively. In the first stage, there was a rapid increase in the voltage and current. In this stage, the growth of the passive oxide film that acts as a barrier layer between the substrate and electrolyte interface occurs at the early deposition stage. In the second stage, the sparks observed around the substrate suggests the breakdown of the passive oxide film formed previously. In this stage, the heating due to the high applied voltage induces the melting of the substrate where the Ti ions and electrons were ejected. The increase in voltage also becomes slower during this stage.

In the final stage, a lower fluctuation of the voltage is observed when the breakdown voltage is reached. The solidification of the melted Ti substrate with the OH^- ions progressively produces a thicker coating resulting in the increase in the coating resistance and hence, larger sparks were observed. The cations and anions from the electrolyte enter into the discharge channel, producing the coating-forming substances. The BG coating growth mechanism and spark observation are illustrated in Figure 2.

The mechanism of oxide coating formation can be described by a series of chemical equations of the electrolyte composition and the Ti substrate. The high voltage during the PEO ionizes the electrolyte composition and substrate material as shown in equations (1) and (2). This ionization of the electrolyte components occurs concurrently during the initial PEO deposition stages.

$$Ti \rightarrow Ti^{4+} + 4e^-, \quad (1)$$

$$NaOH \rightarrow Na^+ + OH^-, \quad (2)$$

$$4OH^- \rightarrow O_2 + 2H_2O + 4e^-, \quad (3)$$

$$O_2 + 2e^- \rightarrow O^{2-}. \quad (4)$$

The BG (45S5) particles in the electrolyte form an ionic matrix in the suspension consisting of the Si^{2+}, Ca^{2+}, Na^{4+}, P^{5+}, and O^{2-} ions. The oxygen released in equation (3) simultaneously leads to the formation of TiO_2 incorporated into the BG particles coating. The oxide coating is formed from the hydroxyl ions and O_2 released from the electrolyte.

$$Ti + 4OH^- \rightarrow TiO_2 + 2H_2O + 4e^-, \quad (5)$$

$$Ti^{4+} + 2O^{2-} \rightarrow TiO_2. \quad (6)$$

The continuous growth of the oxide layer occurs at high potential in the electrolyte. The coating thickens over time due to the ejection of molten Ti through the discharged channels to the surface.

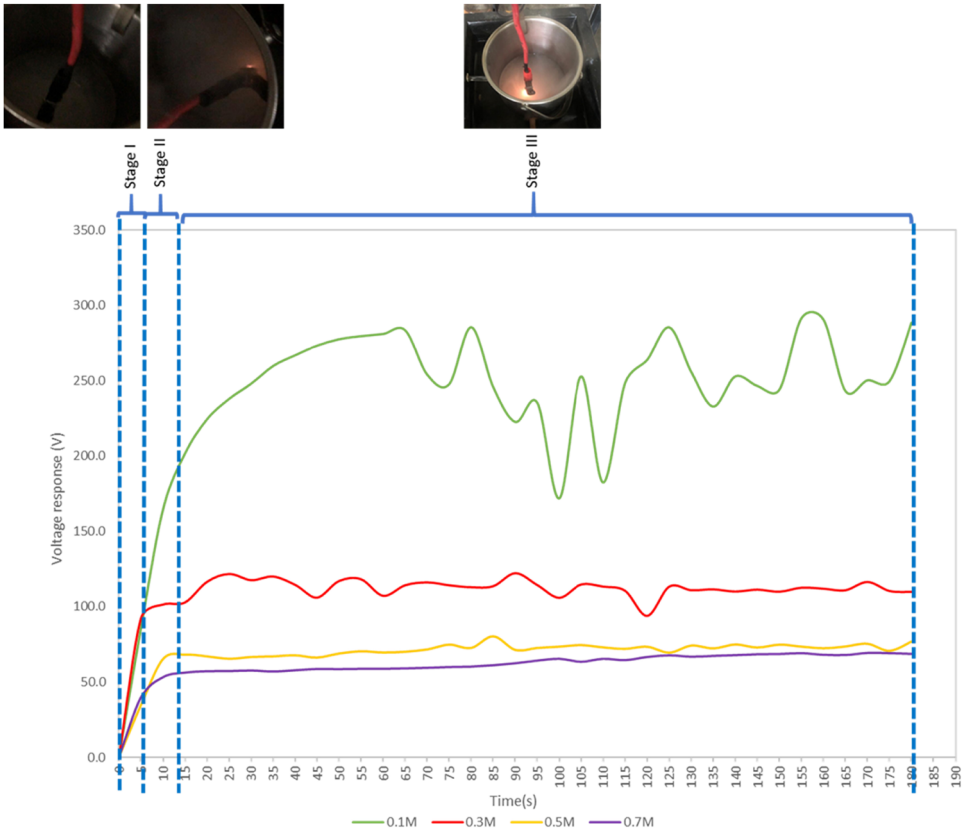

Figure 2: The stages of PEO deposition process.

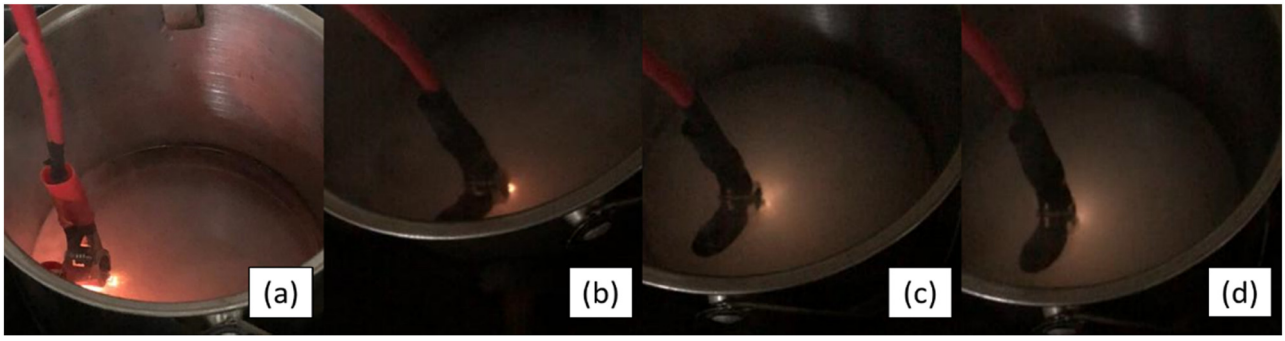

Figure 3: The sparks presence at the substrate during deposition at different NaOH concentrations: (a) 0.1 M, (b) 0.3 M, (c) 0.5 M, and (d) 0.7 M.

3.2 The voltage response during the PEO deposition process

The voltage response recorded on the DC power supply unit interface was recorded and plotted in Figure 2. The voltage response is highly dependent on the NaOH concentration as in the previous reports. This variation of the voltage response could be due to the different amounts of OH^- ions present in the electrolyte.

The different concentrations of NaOH gave different voltage responses. A lower breakdown voltage is achieved with a higher concentration of NaOH. The sparks present during the deposition process decrease with the increase in NaOH concentration as in Figure 3. The lower PEO deposition voltage is attributed to the facile breakdown of the passive oxide film on the substrate due to the large migration of OH^- ions, which subsequently produces dimmer sparks as observed. The lowest concentration of 0.1 M NaOH gave the highest deposition voltage, around 200–250 V. In theory, a higher concentration of NaOH releases a larger amount of OH^- ions which produce a thicker coating as observed on the cross-sectional images of the coating.

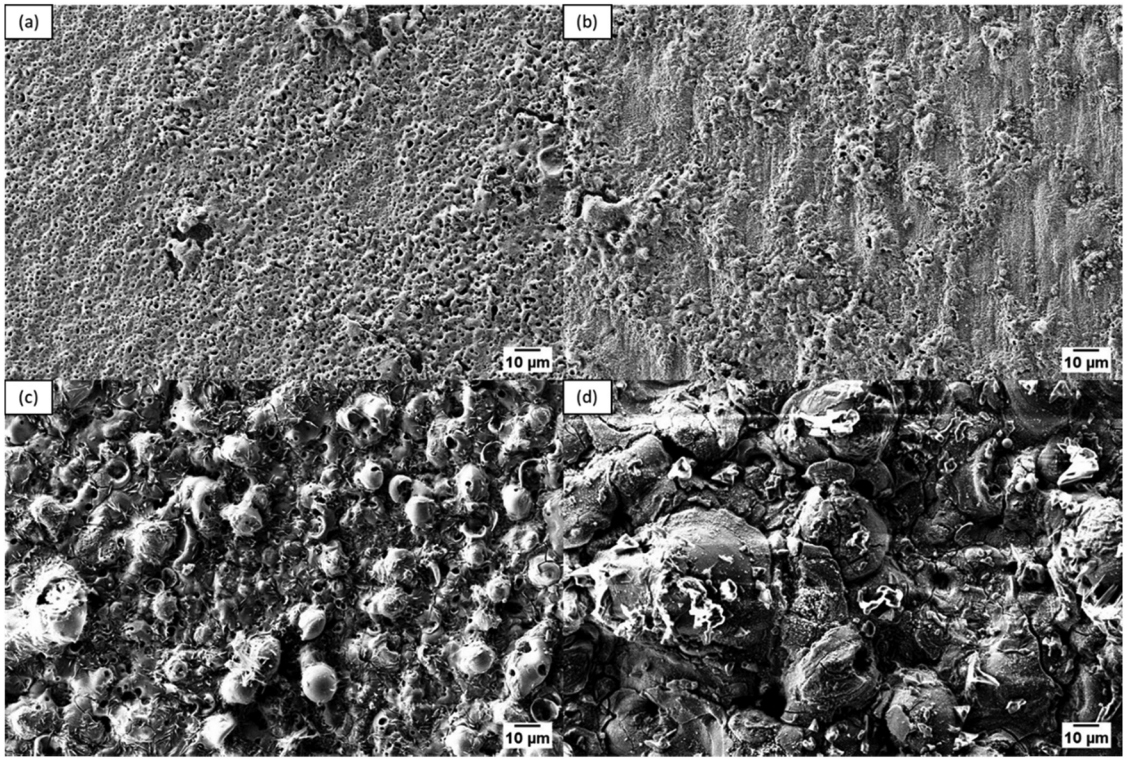

Figure 4: The surface morphology of the coating produced at different NaOH concentrations: (a) 0.1 M, (b) 0.3 M, (c) 0.5 M, and (d) 0.7 M.

3.3 The surface and cross-sectional microstructure and elemental analysis of coating

The surface morphology of the sample was studied with respect to the pore distribution and crack formation. The thickness and the discharge channel of the coating were evaluated by the cross-sectional FESEM images. The coating produced at the lowest concentration (0.1 M) shows a uniform distribution of pores across the substrate, with few thickened spots as observed in Figure 4. However, with the increase in NaOH concentration, the

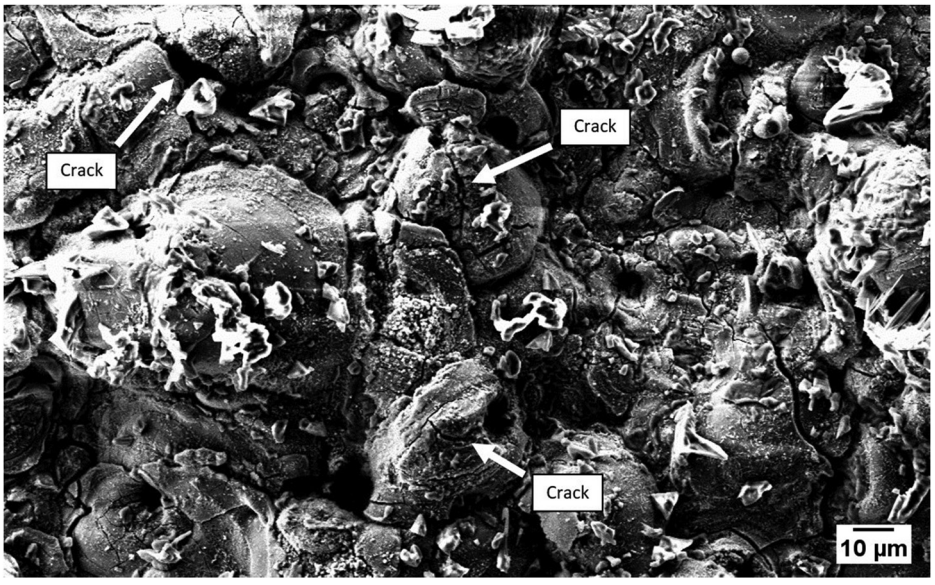

Figure 5: The crack observed on the coating produced at 0.7 M NaOH concentration.

Table 3: The average thickness of coatings produced at different concentrations

Experiment (M)	Average thickness (μm)
0.1	9.5530 ± 5.2462
0.3	17.1167 ± 3.6814
0.5	23.0070 ± 3.4910
0.7	18.1367 ± 3.0936

breakdown of the coating is observed from the irregular thickened spots on the 0.3 M sample and critically formed cracks on the 0.7 M coating, as shown in Figure 5. With the increase in the concentration to 0.5 M and subsequently to 0.7 M, the pores are barely visible as the BG particles completely cover the porous layer.

Cracks are obviously observed on the coating produced at higher concentrations (0.5 and 0.7 M) due to the stress in the inner coating that counters the solidification shrinkage on the outer layer resulting in the micro-cracks and uneven coating. The increase in the temperature localization at the Ti substrate is due to the high potential when the PEO process counterbalances the lower temperature from the cooling bath system, which resulted in the solidification and stress inducement [35]. The rapid solidification during the treatment leads to the formation of a brittle outer coating which resulted in severe coating trackside cracks, as observed along the scratch during the adhesion strength test.

The cross-sectional structure was observed on the sectioned mounted samples. The thickness of the coating was evaluated with respect to each NaOH concentration as shown in Table 3. The coating produced at 0.5 M concentration possesses the thickest coating with dense structure. As the amount of OH^- ions increases with the higher concentrations of NaOH, this subsequently enhances the oxide layer growth according to the reactions described in equations (5) and (6). The increase in the NaOH concentration to 0.7 M contributes to the breakdown of the outer layer coating and large open micropores as observed in the FESEM images in Figure 6. Even though the micropores were barely visible in the surface morphology images, few spots were observed from the cross-sectional images, as shown in Figure 6d. The rapid solidification and melting during the oxide coating formation resulted in the formation of cracks and open micropores. The widely distributed cracks on the outer coating contribute to the serious

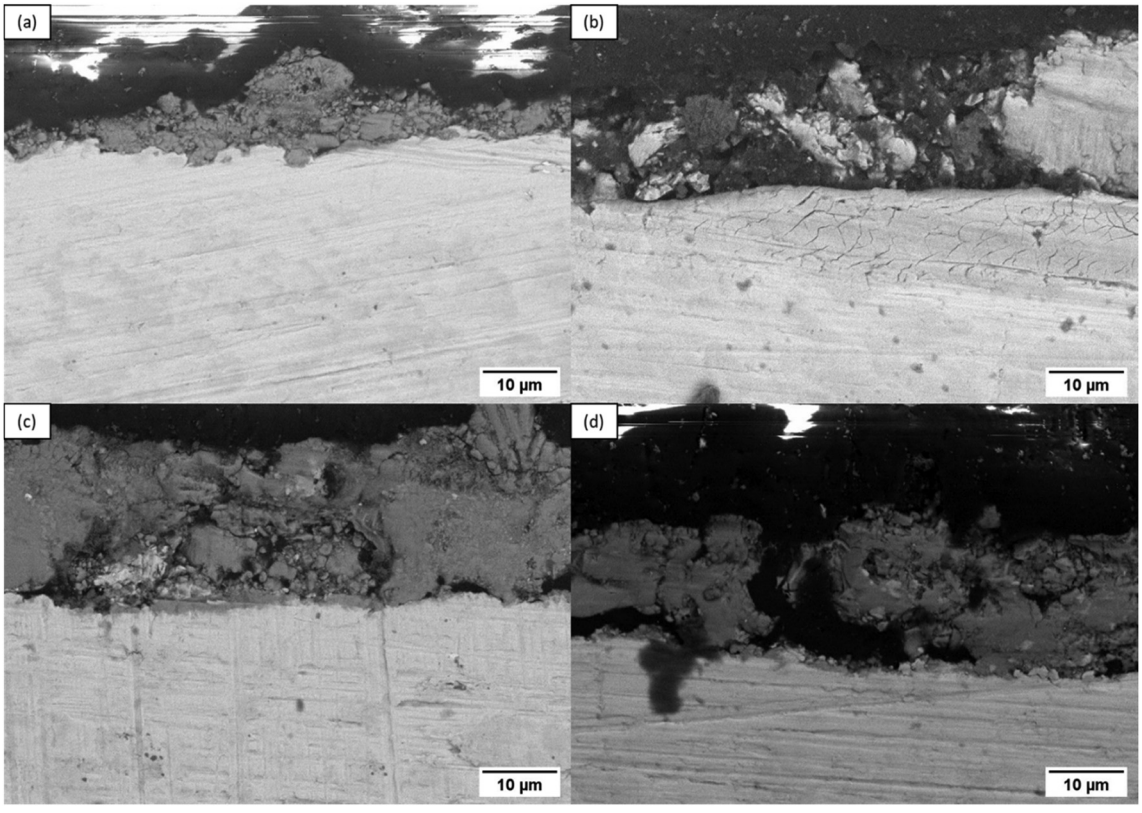

Figure 6: FESEM images of cross-sectional structure of the coating produced at different NaOH concentrations: (a) 0.1 M, (b) 0.3 M, (c) 0.5 M, and (d) 0.7 M.

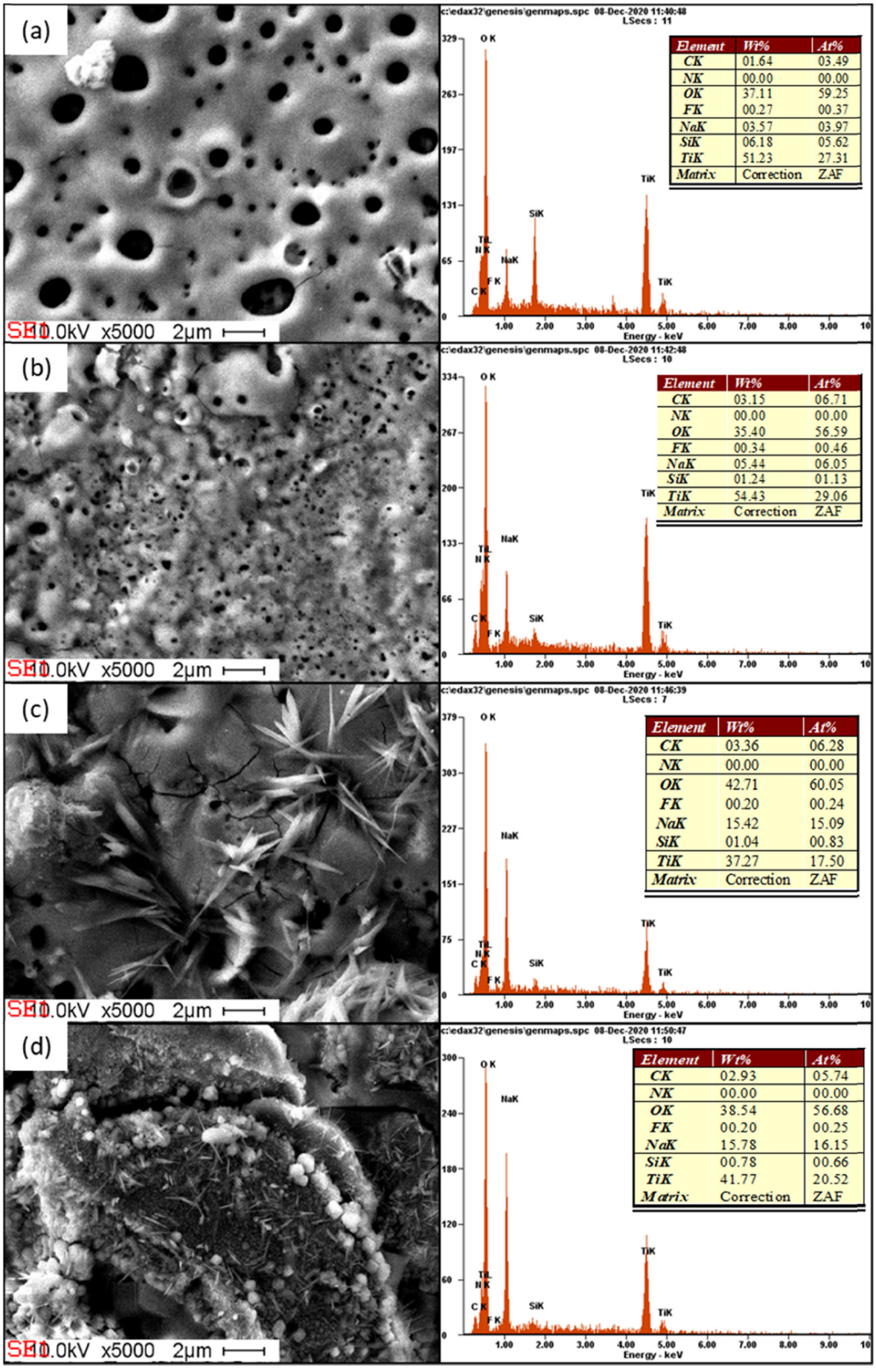

Figure 7: The elemental distribution of the BG incorporated oxide coating produced at (a) 0.1 M, (b) 0.3 M, (c) 0.5 M, and (d) 0.7 M.

trackside cracks as observed during the adhesion strength test track afterward.

The EDS analysis in Figure 7 confirms the incorporation of BG particles into the oxide layer. From the EDS

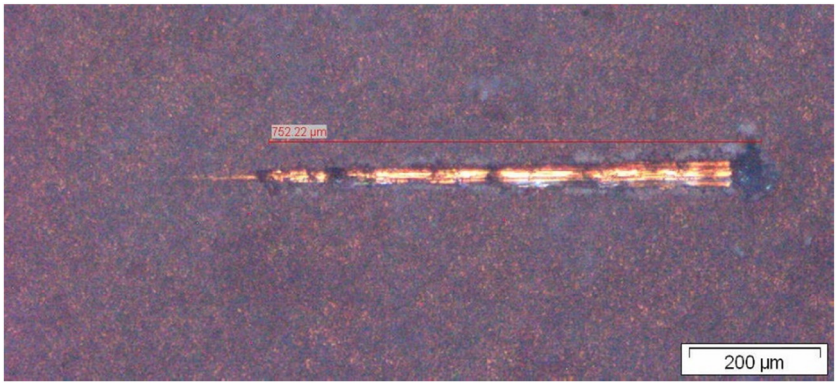

Figure 8: Optical microscope image of the scratch track of the coating produced at 0.1 M NaOH concentration at 5× magnification.

Table 4: The adhesion strength and average hardness of the coating produced at different NaOH concentrations

NaOH concentration (M)	Failure length and critical load (L_{C2})	Average hardness (HV0.3)
0.1	Fails at 247.78 µm with 537.74 mN load	203.25 ± 10.87
0.3	Fails at 305.08 µm with 696.23 mN load	246.25 ± 8.62
0.5	Fails at 324.59 µm with 749.93 mN load	379.00 ± 20.51
0.7	Fails at 607.83 µm with 1531.27 mN load	393.67 ± 16.74

analysis, the higher peak of Ti and oxygen (O) compared to the other elements present in the electrolyte indicates the dominant oxidation of the substrate during the PEO treatment. As observed from the recorded data, the Ti peak gradually decreases with the increase in NaOH concentration due to the deposition of silicon (Si) and sodium (Na) overtaking the molten Ti growth. The Si and Na particles are mainly deposited into the oxide coating as they are the dominant elements in the BG 45S5 composition. The presence of Na also contributes to the increase in the amount of Na observed due to the increase in NaOH concentration; however, the EDS spectrum did not detect the presence of Ca and P elements. This may be due to the smaller amount of these particles present in the 45S5 composition. The relatively lower melting point of the BG (less than 1,200°C) particles may contribute to the failure of these particles being detected by the EDS analysis due to the melting during the PEO process [36]. Furthermore, the deposition of Si and Na into the incorporated oxide layer suggests that the BG particles could be deposited in the oxide layer produced by the PEO treatment in NaOH. The electrochemical reactions in equations (1)–(3) describe the ionization of the BG particles and their subsequent incorporation into the growing oxide layer during the PEO treatment. This demonstrates the workability of PEO to deposit BG particles onto the metal substrate, thus improving the biocompatibility of the substrate material.

3.4 The adhesion strength and hardness of the coating

The micro-scratch test was carried out to evaluate the adhesion strength of the BG incorporated coating produced via the PEO set up. Apart from improving the bioactivity of the Ti implants, the BG incorporated oxide coating also requires excellent mechanical properties. Hence, it is crucial to understand the mechanical properties of the coating when exposed to mechanical stress.

In the micro-scratch test, a linearly increasing load from 0 to 2,000 mN was applied along a 1,000 µm scratch track on four different coatings produced at different NaOH concentrations (0.1, 0.3, 0.5, and 0.7 M). In this study, the failure point of each coating was evaluated with respect to the distance where the coating delaminates completely exposing the substrate. The BG incorporated oxide coating produced at the lowest NaOH concentration (0.1 M) exhibits the lowest adhesion strength with a failure point at 247.78 µm with 537.74 mN applied load, as shown in Figure 8. Table 4 shows the results of each scratch test and hardness test on the coatings produced at different NaOH concentrations. The results show an increase in the adhesion strength and hardness with the increase in the NaOH concentration. This trend is attributed by the denser coating produced at higher concentration which subsequently improves the adhesion strength of the BG incorporated coating. The high

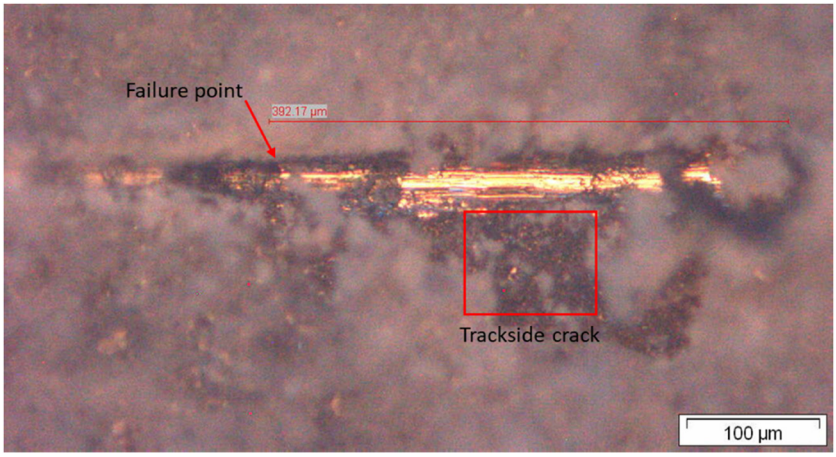

Figure 9: Optical microscope image of the delamination of coating produced at 0.7 M concentration at 10× magnification.

concentration of OH^- ions form thicker layers based on the chemical reaction, equations (5) and (6) occurring in the electrolyte. The thicker coating produced contributes to the improved hardness of the BG incorporated oxide layer. Although the adhesion strength increases with the NaOH concentration, the severe trackside cracks of the coating was also observed along the scratch track as shown in Figure 9. The formation of cracks in the outer coating and also the large discharge channel as observed in the morphology and cross-sectional images contribute to the facile trackside cracks of the coating.

3.5 Bioactivity of the coating

The bioactivity of the coating was evaluated by the apatite forming ability of the PEO coating. In order to test the ability of the coating to induce the apatite layer formation, the coated sample was immersed in the SBF and incubated for 14 days at a constant temperature of 37°C. This procedure was done in order to confirm the apatite inducing ability of the BG incorporated coating, which subsequently demonstrates the feasibility of the PEO method in producing a BG incorporated bio-functional coating.

The morphology of the immersed coated sample was analysed by FESEM to confirm the formation of a new apatite layer. From the FESEM images, a scabrous structured layer was observed on the first BG incorporated layer produced by the PEO. The presence of the scabrous layer which shields the previously formed BG incorporated PEO coating confirms the formation of an apatite layer during the SBF immersion, Figure 10.

The incorporation of the BG particles into the coatings confirms the successful formation of an apatite layer.

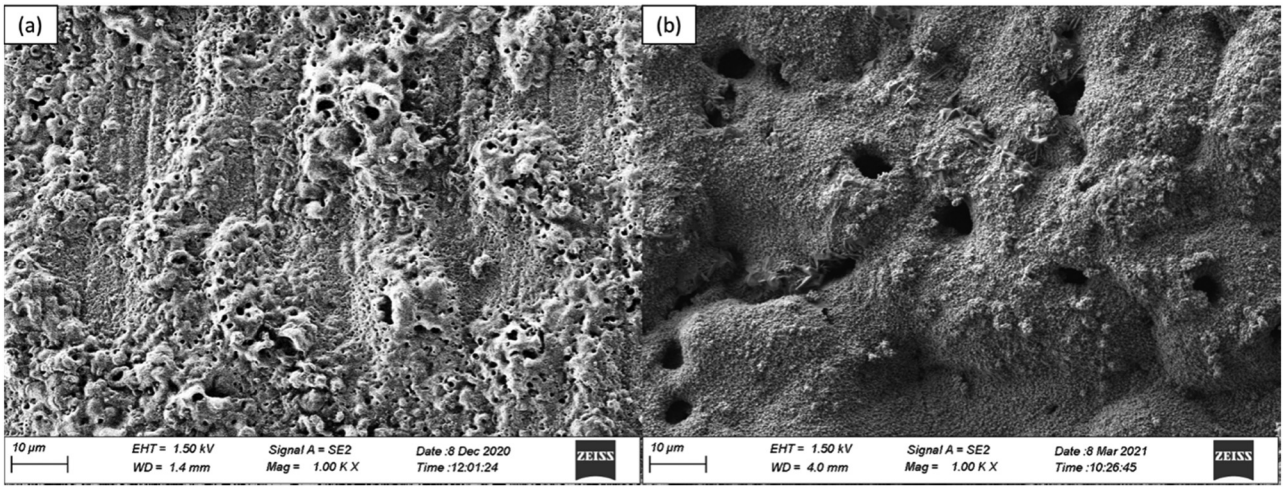

Figure 10: FESEM images of 0.3 M coating at 1,000× magnification of bioglass incorporated coating: (a) prior to SBF immersion and (b) after the SBF immersion for 14 days.

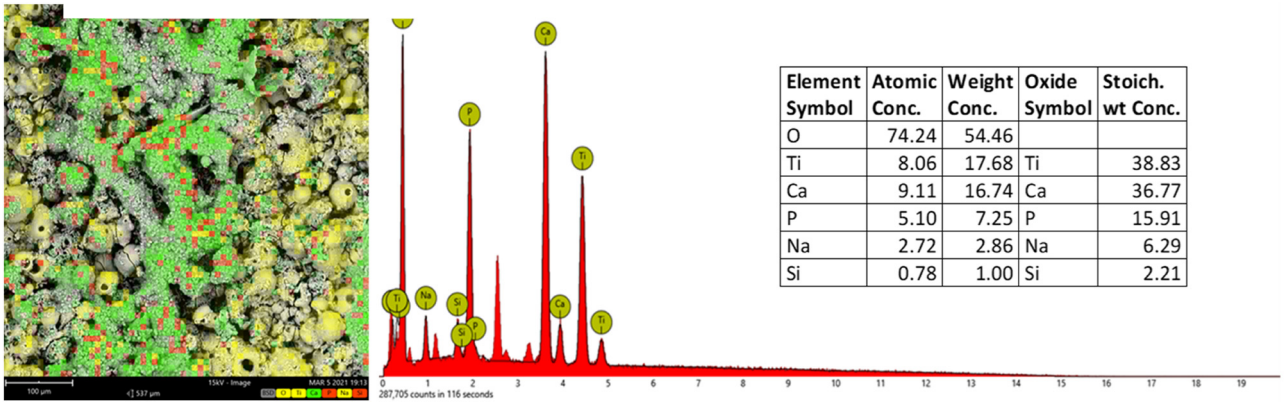

Element Symbol	Atomic Conc.	Weight Conc.	Oxide Symbol	Stoich. wt Conc.
O	74.24	54.46		
Ti	8.06	17.68	Ti	38.83
Ca	9.11	16.74	Ca	36.77
P	5.10	7.25	P	15.91
Na	2.72	2.86	Na	6.29
Si	0.78	1.00	Si	2.21

Figure 11: The EDS spectrum of SBF immersed coating.

The Ca/P ratio was obtained from the EDS spectrum of the formed apatite layer. The SBF-immersed samples illustrate a Ca/P ratio of 1.79, close to the pure apatite (1.67), Figure 11. The ratio of the Ca/P and the elements detected in the apatite layer may confirm the bio-functional coating ability to induce the bond formation between the bone/tissues and the implant surface. The apatite layer caused on the BG coating demonstrates the feasibility of the PEO technique to incorporate a bio-functional property on the Ti substrate, thus enhancing the biocompatibility of the Ti alloy as a medical implant material.

4 Conclusion

The increase in the NaOH electrolyte concentration gives a significant variation on the mechanical properties of the coated sample. The thickness and mechanical properties of the coating improve with the increase in the NaOH concentration, despite the severe delamination of the coating and widely distributed cracks on the surface. The increase in the OH^- ion concentration in the electrolyte enhances the growth of thicker oxide coatings. However, increasing the NaOH concentration to 0.7 M induces the breakdown of the coating and leads to the severe trackside cracks of the coating. Hence, it is crucial to obtain the optimum process parameter for a coating with excellent mechanical properties and uniformly distributed BG particles for ideal bioactive properties.

Acknowledgements: The authors would like to acknowledge the facilities and resources provided by the Universiti Malaya for the completion of this project.

Funding information: This project was supported by the FRGS grant (No. FRGS/1/2018/TK05/UM/01/2), awarded by the Ministry of Higher Education (MOHE) Malaysia.

Author contributions: Conceptualization: A.R. Bushroa; experimentation and methodology: A.R. Bushroa and N.A. Sukrey; analysis and investigation: N.A. Sukrey and A.R. Bushroa; writing – first draft preparation: N.A. Sukrey; writing – review and improvements: M. Rizwan, S.Z. Salleh, and W.J. Basirun; writing – revisions and rebuttal to reviewer: M. Rizwan, S.Z. Salleh, W.J. Basirun, and A.R. Bushroa; supervision: A.R. Bushroa; and funding acquisition: A.R. Bushroa.

Conflict of interest: Authors state no conflict of interest.

Data availability statement: All data generated or analyzed during this study are already included in this published article.

References

[1] Kurup, A., P. Dhatrak, and N. Khasnis. Surface modification techniques of titanium and titanium alloys for biomedical dental applications: A review. *Materials Today: Proceedings*, Vol. 39, No. 1, 2020, pp. 84–89.

[2] Quintero, D., O. Galvis, J. A. Calderón, J. G. Castaño, and F. Echeverría. Effect of electrochemical parameters on the formation of anodic films on commercially pure titanium by plasma electrolytic oxidation. *Surface and Coatings Technology*, Vol. 258, 2014, pp. 1223–1231.

[3] Rack, H. J. and J. I. Qazi. Titanium alloys for biomedical applications. *Materials Science & Engineering, C: Materials for Biological Applications*, Vol. 26, 2006, pp. 1269–1277.

[4] Schenk, R. The corrosion properties of titanium and titanium alloys BT – titanium in medicine: material science. In Brunette D. M., P. Tengvall, M. Textor, and P. Thomsen, eds., *Surface science, engineering, biological responses and medical applications*. Springer Berlin Heidelberg, Berlin, Heidelberg, 2001, pp. 145–170.

[5] Liu, W., S. Liu, and L. Wang. Surface modification of biomedical titanium alloy: Micromorphology, microstructure evolution and biomedical applications. *Coatings*, Vol. 9, 2019, id. 249.

[6] Necula, B. S., I. Apachitei, L. E. Fratila-Apachitei, E. J. Van Langelaan, and J. Duszczyk. Titanium bone implants with superimposed micro/nano-scale porosity and antibacterial capability. *Applied Surface Science*, Vol. 273, 2013, pp. 310–314.

[7] Pereira, B. L., C. M. Lepienski, I. Mazzaro, and N. K. Kuromoto. Apatite grown in niobium by two-step plasma electrolytic oxidation. *Materials Science & Engineering, C: Materials for Biological Applications*, Vol. 77, 2017, pp. 1235–1241.

[8] Xing, F., C. Zhou, D. Hui, C. Du, L. Wu, L. Wang, et al. Hyaluronic acid as a bioactive component for bone tissue regeneration: Fabrication, modification, properties, and biological functions. *Nanotechnology Reviews*, Vol. 9, 2020, pp. 1059–1079.

[9] Łępicka, M. and M. Grądzka-Dahlke. The initial evaluation of performance of hard anti-wear coatings deposited on metallic substrates: thickness, mechanical properties and adhesion measurements – a brief review. *Reviews on Advanced Materials Science*, Vol. 58, 2019, pp. 50–65.

[10] Sedelnikova, M. B., E. G. Komarova, Y. P. Sharkeev, A. V. Ugodchikova, T. V. Tolkacheva, J. V. Rau, et al. Modification of titanium surface via Ag-, Sr- and Si-containing micro-arc calcium phosphate coating. *Bioactive Materials*, Vol. 4, 2019, pp. 224–235.

[11] Cordeiro, J. M., B. E. Nagay, A. L. R. Ribeiro, N. C. da Cruz, E. C. Rangel, L. M. G. Fais, et al. Functionalization of an experimental Ti-Nb-Zr-Ta alloy with a biomimetic coating produced by plasma electrolytic oxidation. *Journal of Alloys and Compounds*, Vol. 770, 2019, pp. 1038–1048.

[12] Ragel, C. V., M. Vallet-Regí, and L. M. Rodríguez-Lorenzo. Preparation and *in vitro* bioactivity of hydroxyapatite/solgel glass biphasic material. *Biomaterials*, Vol. 23, 2002, pp. 1865–1872.

[13] Cai, S., C. Wu, W. Yang, W. Liang, H. Yu, and L. Liu. Recent advance in surface modification for regulating cell adhesion and behaviors. *Nanotechnology Reviews*, Vol. 9, 2020, pp. 971–989.

[14] Nakonieczny, D. S., M. Antonowicz, and Z. Paszenda. Surface modification methods of ceramic filler in ceramic-carbon fibre composites for bioengineering applications – A systematic review. *Reviews on Advanced Materials Science*, Vol. 59, 2020, pp. 586–605.

[15] Balestriere, M. A., K. Schuhladen, K. Herrera Seitz, A. R. Boccaccini, S. M. Cere, and J. Ballarre. Sol-gel coatings incorporating borosilicate bioactive glass enhance anti corrosive and surface performance of stainless steel implants. *Journal of Electroanalytical Chemistry*, Vol. 876, 2020, id. 114735.

[16] Rizwan, M., M. Hamdi, and W. J. Basirun. Bioglass® 45S5-based composites for bone tissue engineering and functional applications. *Journal of biomedical materials research. Part A*, Vol. 105, 2017, pp. 3197–3223.

[17] Moriche, R., A. M. Beltrán, B. Begines, J. A. Rodríguez-Ortiz, A. Alcudia, and Y. Torres. Influence of the porosity and type of bioglass on the micro-mechanical and bioactive behavior of coated porous titanium substrates. *Journal of Non-Crystalline Solids*, Vol. 551, 2021, id. 120436.

[18] Fernandes, H. R., A. Gaddam, A. Rebelo, D. Brazete, G. E. Stan, and J. M. F. Ferreira. Bioactive glasses and glass-ceramics for healthcare applications in bone regeneration and tissue engineering. *Materials* (*Basel*), Vol. 11, 2018, id. 2530.

[19] Tabia, Z., S. Akhtach, K. El Mabrouk, M. Bricha, K. Nouneh, and A. Ballamurugan. Tantalum doped SiO2-CaO-P2O5 based bioactive glasses: Investigation of *in vitro* bioactivity and antibacterial activities. *Biomedical Glasses*, Vol. 6, 2020, pp. 10–22.

[20] Rohr, N., J. B. Nebe, F. Schmidli, P. Müller, M. Weber, H. Fischer, et al. Influence of bioactive glass-coating of zirconia implant surfaces on human osteoblast behavior *in vitro*. *Dental Materials*, Vol. 35, 2019, pp. 862–870.

[21] Yang, W., D. Xu, T. Chen, J. Wang, and J. Chen. Microstructure and photocatalytic performance of micro arc oxidation coatings after heat treatment. *Science and Engineering of Composite Materials*, Vol. 27, 2020, pp. 19–27.

[22] Adeleke, S. A., S. Ramesh, A. R. Bushroa, Y. C. Ching, I. Sopyan, M. A. Maleque, et al. The properties of hydroxyapatite ceramic coatings produced by plasma electrolytic oxidation. *Ceramics International*, Vol. 44, 2018, pp. 1802–1811.

[23] Rizwan, M., R. Alias, U. Z. Zaidi, R. Mahmoodian, and M. Hamdi. Surface modification of valve metals using plasma electrolytic oxidation for antibacterial applications: A review. *Journal of Biomedical Materials Research Part A*, Vol. 106, 2018, pp. 590–605.

[24] Souza, J. G. S., M. M. Bertolini, R. C. Costa, B. E. Nagay, A. Dongari-Bagtzoglou, and V. A. R. Barão. Targeting implant-associated infections: Titanium surface loaded with antimicrobial. *IScience*, Vol. 24, 2021, id. 102008.

[25] Costa, R. C., J. G. S. Souza, J. M. Cordeiro, M. Bertolini, E. D. de Avila, R. Landers, et al. Synthesis of bioactive glass-based coating by plasma electrolytic oxidation: Untangling a new deposition pathway toward titanium implant surfaces. *Journal of Colloid and Interface Science*, Vol. 579, 2020, pp. 680–698.

[26] Oliver, J. N., Y. Su, X. Lu, P.-H. Kuo, J. Du, and D. Zhu. Bioactive glass coatings on metallic implants for biomedical applications. *Bioactive Materials*, Vol. 4, 2019, pp. 261–270.

[27] Lu, X., M. Mohedano, C. Blawert, E. Matykina, R. Arrabal, K. U. Kainer, et al. Plasma electrolytic oxidation coatings with particle additions – A review. *Surface Coatings Technology*, Vol. 307, 2016, pp. 1165–1182.

[28] Kaseem, M., S. Fatimah, N. Nashrah, and Y. G. Ko. Recent progress in surface modification of metals coated by plasma electrolytic oxidation: Principle, structure, and performance. *Progress in Materials Science*, Vol. 117, 2021, id. 100735.

[29] Luo, S., Q. Wang, R. Ye, and C. S. Ramachandran. Effects of electrolyte concentration on the microstructure and properties of plasma electrolytic oxidation coatings on Ti-6Al-4V alloy. *Surface Coatings Technology*, Vol. 375, 2019, pp. 864–876.

[30] Krupa, D., J. Baszkiewicz, B. Rajchel, A. Barcz, J. W. Sobczak, and A. Biliński. Effect of sodium-ion implantation on the

corrosion resistance and bioactivity of titanium. *Vacuum*, Vol. 78, 2005, pp. 161–166.
[31] Farooq, I., Z. Imran, U. Farooq, M. A. Leghari, and H. Ali. Bioactive glass: A material for the future. *World Journal of Dentistry*, Vol. 3, 2012, pp. 199–201.
[32] Maitz, M. F., R. W. Y. Poon, X. Y. Liu, M.-T. Pham, and P. K. Chu. Bioactivity of titanium following sodium plasma immersion ion implantation and deposition. *Biomaterials*, Vol. 26, 2005, pp. 5465–5473.
[33] Kokubo, T. and H. Takadama. How useful is SBF in predicting *in vivo* bone bioactivity? *Biomaterials*, Vol. 27, 2006, pp. 2907–2915.
[34] Kokubo, T., H. Kushitani, S. Sakka, T. Kitsugi, and T. Yamamuro. Solutions able to reproduce *in vivo* surface-structure changes in bioactive glass-ceramic A-W3. *Journal of Biomedical Materials Research*, Vol. 24, 1990, pp. 721–734.
[35] Zakaria, A., H. Shukor, M. Todoh, and K. Jusoff. Bio-functional coating on Ti6Al4V surface produced by using plasma electrolytic oxidation. *Metals* (*Basel*), Vol. 10, 2020, id. 1124.
[36] Lu, X., M. Mohedano, C. Blawert, E. Matykina, R. Arrabal, K. U. Kainer, et al. Plasma electrolytic oxidation coatings with particle additions – A review. *Surface Coatings Technology*, Vol. 307, 2016, pp. 1165–1182.